NANO LETTERS
Cite This: Nano Lett. 2019, 19, 612–617
Letter
pubs.acs.org/NanoLett

Ultra-Sensitive and Label-Free Probing of Binding Affinity Using Recognition Imaging

Yoo Jin Oh,[†] Melanie Koehler,[†,§] Yoonhee Lee,[‡,∥] Sourav Mishra,[‡] Joon Won Park,[‡] and Peter Hinterdorfer*[,†]

[†]Institute of Biophysics, Johannes Kepler University Linz, Gruberstrasse 40, A-4020 Linz, Austria

[‡]Department of Chemistry, Pohang University of Science and Technology, 77 Cheongam-Ro, Nam-Gu, Pohang 37673, Republic of Korea

Supporting Information

ABSTRACT: Reliable quantification of binding affinity is important in biotechnology and pharmacology and increasingly coupled with a demand for ultrasensitivity, nanoscale resolution, and minute sample amounts. Standard techniques are not able to meet these criteria. This study provides a new platform based on atomic force microscopy (AFM)-derived recognition imaging to determine affinity by visualizing single molecular bindings on nanosize dendrons. Using DNA hybridization as a demonstrator, an AFM sensor adorned with a cognate binding strand senses and localizes target DNAs at nanometer resolution. To overcome the limitations of speed and resolution, the AFM cantilever is sinusoidally oscillated close to resonance conditions at small amplitudes. The equilibrium dissociation constant of capturing DNA duplexes was obtained, yielding 2.4×10^{-10} M. Our label-free single-molecular biochemical analysis approach evidences the utility of recognition imaging and analysis in quantifying biomolecular interactions of just a few hundred molecules.

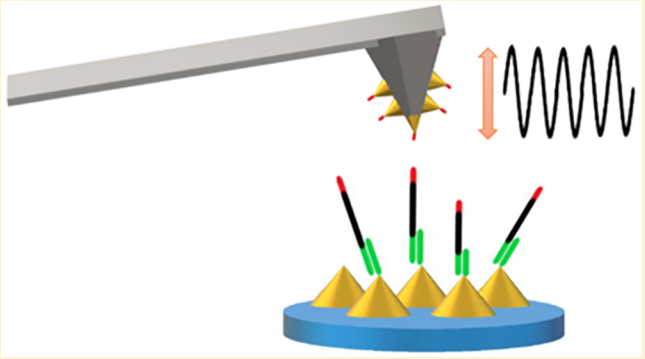

KEYWORDS: *Affinity, single-molecule, scanning probe microscopy, molecular recognition, DNA hybridization*

The replacement of traditional bioassays, including DNA microarrays and ELISA, is highly demanded for the development of high-accuracy tests in molecular diagnostics. Single-molecule bioassays have become increasingly important for disease diagnosis, genome research, personalized medicine, and pharmaceutical research. Fast and direct measurement of the equilibrium dissociation constant (K_D) is challenging because labeling is essential to read or amplify single molecular binding events. Microarrays[1,2] and enzyme-linked immunosorbent assays (ELISAs)[3,4] rely on fluorescence tags and/or labeling,[5,6] which can result in short fluorophore life times coupled with high noise.[4,5] Digital ELISA,[4] nanoparticle-based biobarcode assay,[7] and Förster resonance energy transfer (FRET)[6] have been emerged as a sensitive tools for studying single-molecule affinity. However, delicate steps are required to engineer the beads (or nanoparticles), coat them with an optimized molecule density, and attach labels to the probe and target molecules.[2,7] Kinetic analysis by FRET enables the detection of single-molecule interactions through a single pair of fluorophores at sufficient temporal resolution. However, in addition to photobleaching, FRET signals can be interfered by nonspecific binding events from adjacent molecules, inducing errors in the quantification of the equilibrium dissociation constant (K_D) value.[5,6] Label-free methods[8−11] such as surface plasmon resonance (SPR) and quartz crystal microbalance (QCM) rely on mass detection, and characterizing small-molecule binding is particularly challenging.

We derived a sensitive, label-free, and fast affinity measurement tool from the combination of topography imaging and force spectroscopy,[12] which is a versatile tool for the specific recognition and localization of single biomolecules at the nanoscale. AFM topography imaging allows the resolution of the surface structure of individual biomolecules[13] such as proteins, DNA, and peptides with nanometer resolution, whereas force spectroscopy is sufficiently sensitive to measure pico-Newton ranges of forces on the single molecular level to discern molecular elasticity,[14] stiffness,[15] and adhesion[16,17] as well as ligand−receptor interaction[18−21] and protein unfolding.[22,23] Here, we perform a DNA assay to quantify target DNAs captured on a substrate structured with complementary DNA.

We employ a *BCR-ABL* gene, a biomarker of chronic myeloid leukemia[24] as the target (170-mer), and a capture DNA probe that was designed to bind a translocated junction of the *BCR-ABL* strand (40-mer) (Figure 1). Dendron-coated

Received: December 6, 2018
Revised: December 17, 2018
Published: December 18, 2018

DOI: 10.1021/acs.nanolett.8b04883
Nano Lett. 2019, 19, 612−617

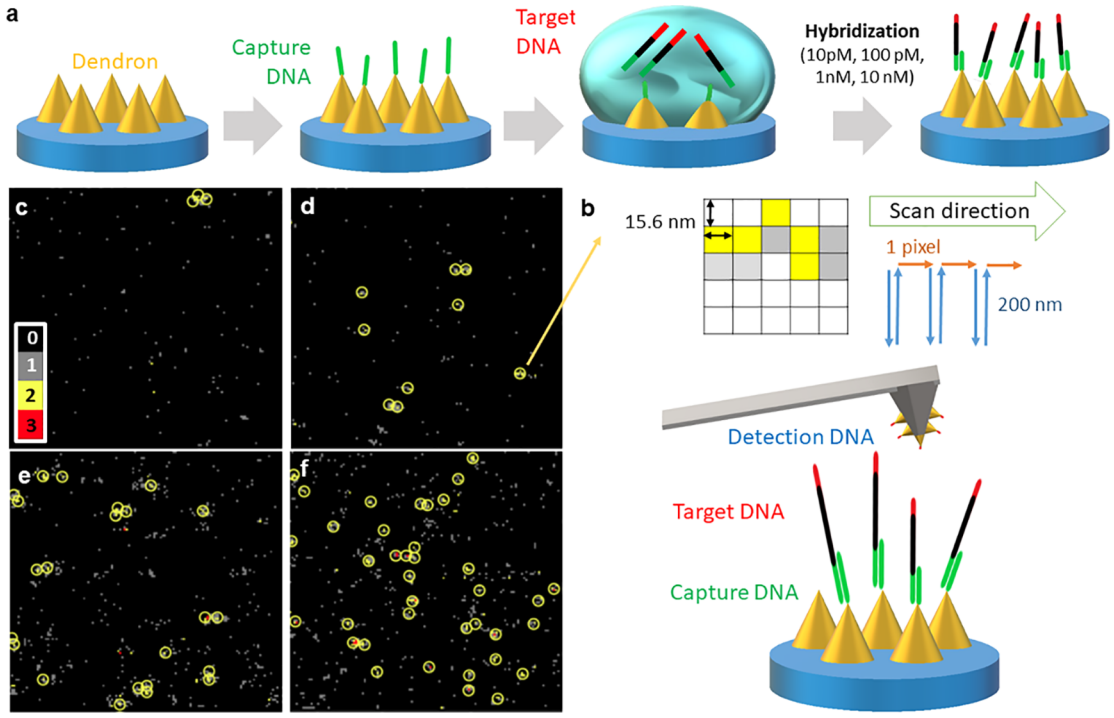

Figure 1. Design of the DNA sensing platform and force−distance-based force mapping. (a) DNA fabricated on a dendron-coated surface, rendering mesospacing between immobilized capture DNAs.[39] Target DNA hybridization is generated by injecting 90 μL of target DNA solution at 4 different concentrations, i.e., 1.0×10^1 pM, 1.0×10^2 pM, 1.0 nM, and 1.0×10^1 nM. (b) Sketch of force-mapping operation. Magnified image of a circled area in panel d; hybridization regions are indicated in yellow. (c−f) Overlaid force maps from three consecutive experiments after hybridization with different concentrations of (c) 1.0×10^1 pM, (d) 1.0×10^2 pM, (e) 1.0 nM, and (f) 1.0×10^1 nM of target DNA. Colors (as indicated in the panel c inset) depict the number of specific unbinding events per pixel detected from three force maps. All images are taken in a 2 μm × 2 μm area with 128 pixels × 128 pixels (15.6 nm pixel size).

Table 1. Sequences of Capture, Target, and Detection Oligonucleotides[a]

Species	Sequence
Detection DNA (20 mer)	5'-/5AmMC6/ GTG CAG AGT GGA GGG AGA AC -3'
Target DNA (170 mer)	5'- TGC TAC TGG CCG CTG AAG GGC TTC TTC CTT ATT GAT GGT CAG CGG AAT GCT GTG GAC AGT CTG GAG TTT CAC ACA CGA GTT GGT CAG CAT CTG CAG CTC CAC GGA TGT CAG GGA GAA GCT TCT GAA ACA CTT CTT CTG CTG CTC CCG GAT GTT CTC CCT CCA CTC TGC AC -3'
Capture DNA (40 mer)	5'- GAC CAT CAA TAA GGA AGA AGC CCT TCA GCG GCC AGT AGC A/3AmM/-3'

[a]Complementary sequences capable for hybridization are marked in colors.

silicon substrates provide lateral spacing between the tether site of the capture DNAs, improving the hybridization efficiency of the target DNA[25] (Figure 1a). It was also shown that the use of such substrates enhances the single-nucleotide polymorphism discrimination efficiency of DNA capture probes, resulting in selectivity as high as 100:1.[25] If necessary, a modified capture probe can be employed for the further enhanced selectivity. For example, locked nucleic acid probes on the surface were able to capture BCR-ABL transcripts specifically, even in the presence of a million copies of normal BCR and ABL genes.[26] Detection DNA is tethered to an AFM tip designed to hybridize the other end region of target DNA (20-mer). (Figure 1b). Sequences of capture, target, and detection DNA are outlined in Table 1. This nanoscale detection platform has been established by a conventional two-dimensional force-mapping approach, demonstrating a sensitivity of fewer than 10 copies of target DNA.[27] Utilizing the specific hydrodynamic distance of the bound DNA duplex as a signature, this approach enables the localization and quantification of the target DNA occupied on the probe spot. After hybridization of the target DNA to the substrate, the interaction between tip-bound detection DNA and target DNA is monitored by reading the mechanical unbinding force through a vertical static off-resonance cantilever movement (frequency of 4 Hz and 200 nm amplitude) in each image pixel (pixel size of 15.6 nm) (Figure 1b). We collected force−distance curves in 128 pixels × 128 pixels from three consecutive force maps of the same area (70

DOI: 10.1021/acs.nanolett.8b04883
Nano Lett. 2019, 19, 612−617

Table 2. Quantification of Detected Target DNA with TREC Imaging (1st Row) and Force Mapping (2nd Row)

target DNA concentration in solution	1.0×10^1 pM	1.0×10^2 pM	1.0 nM	1.0×10^1 nM
recognition pixels (%)	3.64 ± 0.65 (n = 10)	6.51 ± 2.05 (n = 8)	19.07 ± 2.59 (n = 5)	21.83 ± 2.86 (n = 8)
number of clusters	3	9	23	38

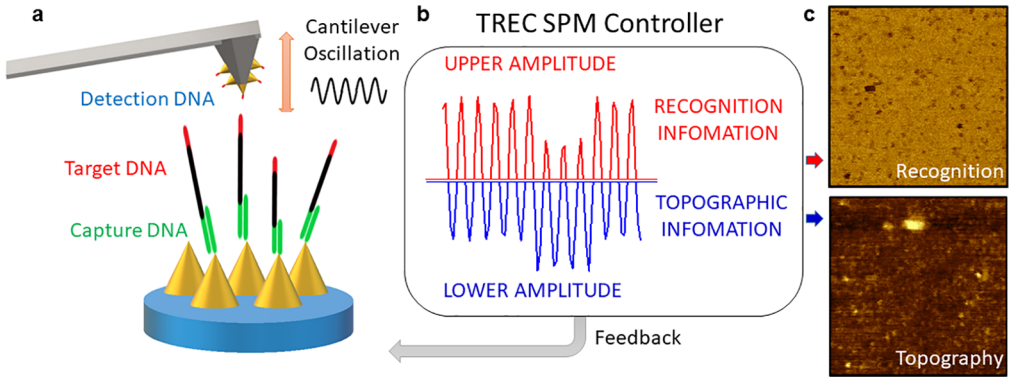

Figure 2. DNA detection based on topography and recognition (TREC) imaging. (a) A cantilever functionalized with a cognate-detection DNA strand is oscillated across the DNA platform, allowing the binding of the detection DNA to the surface-immobilized target DNA. (b) Cantilever oscillations are continuously recorded. Recognition information is depicted solely from the upper oscillation peaks and topography information solely from the lower peaks. (c) Peak signals are fed into the SPM controller, from which the recognition and topography images are constructed. Single-target DNA molecules are visible as dark spots in the recognition image.

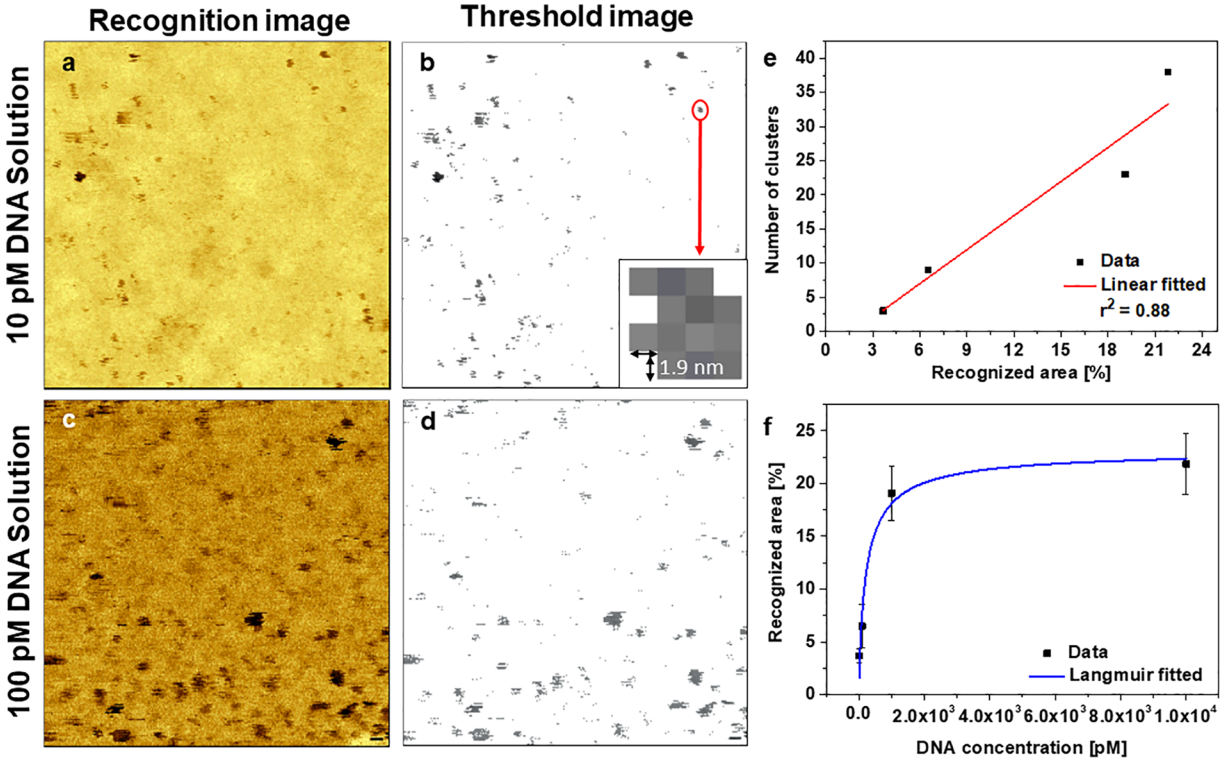

Figure 3. Affinity determination of DNA hybridization recognition images depicting detection of capture DNA hybridized to surface-bound target DNA. (a, b) 1.0×10^1 pM target DNA: (a) recognition image and (b) voltage-threshold-marked recognition image. (c, d) 1.0×10^2 pM target DNA: (c) recognition image and (d) voltage-threshold-marked recognition image. (b, d) Individual grains are generated with a voltage threshold setting of 0.5 V (background noise) when the peak to peak amplitude was set to 1.5 V. The voltage threshold gains for each image are collected and the number of pixels containing a recognition signal over the total number of pixels is calculated to assess the percentage of recognition pixels in the scanned area. All images are 500 nm × 500 nm in an area recorded at 256 pixels × 256 pixels (1.9 nm pixel size). Inset: magnified image of a circled area in panel b. (e) Percentage of recognition pixels obtained with TREC vs number of clusters measured by force mapping. (f) Plot of total recognition pixels area vs target DNA concentration fitted with the Langmuir isotherm model.

min per one real map). After filtering data from each pixel with defined values of stretching distance (10−40 nm) and unbinding force (20−40 pN), we then generated an overlaid map with evaluated pixels containing specific force−distance curves after lateral drift correction.[28] From the overlaid map, pixels showing two or three specific unbinding events are

DOI: 10.1021/acs.nanolett.8b04883
Nano Lett. 2019, 19, 612−617

colored in yellow or red, and pixels containing a single or no specific unbinding event appear in gray or black, respectively (Figure 1c–f). Thereafter, interaction clusters with a size exceeding the hydrodynamic detection radius (29.9 nm)[26] that show more than two times specific unbinding events are counted (Table 2). As we raise the application of the DNA target concentration from 10 pM to 10 nM, the number of specific clusters increases from 3 to 38 per 2.0 μm × 2.0 μm area (Figure 1c–f and Table 2).

Although the force-mapping method allows the direct quantification of the bound target DNAs on the surface at the single-molecule level, the throughput of high-resolution force mapping is still demanding. Simultaneous topography and recognition imaging (TREC)[29−31] enables a fast mapping of biomolecular recognition events on biological surfaces, including the cell membrane.[32] To overcome the limitations of speed and resolution, the AFM cantilever is sinusoidally oscillated at small amplitudes (~8 nm) and close to resonance conditions at a fixed frequency (~10 kHz). The AFM tip senses the surface during lateral scans to simultaneously record topography images and localize specific binding sites at a nanometer accuracy (Figure 2). Amplitude oscillation changes arising from tip−surface interactions are depicted and split into lower and upper parts. From these signals, topographical and recognition images are constructed, respectively (Figure 2b).[33] When the tip-adorned detection DNA binds to the target DNA placed on the silicon substrate, solely the upper parts of the oscillating amplitude are reduced as a result of specific recognition. Thus, upper movements of the cantilever are extenuated when a hybridization between detection and target DNA is established because the AFM tip is temporarily bridged to the surface. These interactions are localized and presented as dark spots in the recognition image (Figure 2c). Each pixel has a size of 1.9 nm and is sensed 20 times by the oscillating cantilever, from which averaged data are generated. An image containing 256 pixels × 256 pixels is taken within 4.25 min.

We then provide adequate control experiments to evaluate the specificity and robustness of our recordings. Because setting the oscillation amplitude of the cantilever is crucial, it can be used as a quick and inherent specificity control without perturbation of the DNA analytes.[33] If well-adjusted, the DNA duplex that forms between tip and surface exerts a non-negligible force influence to the cantilever. Then the top peaks of the cantilever oscillations generate well-defined recognition spots (Figure S1a, arrow) with sufficient background rejection. Under optimized conditions, the detection DNA adorned to the tip and the target DNA bound to the surface form a bond until the tip is laterally moved away from the target DNA to finally break the complex. In contrast, too large of an oscillation amplitude leads to breaking of the DNA complex at each oscillation cycle. In this case, no clearly detectable recognition spots are recorded, as shown (Figure S1b,c). In addition, blocking experiments unequivocally validate that the measured recognition events are due to specific molecular binding of the detection DNA to the target DNA. When we inject a single-stranded DNA designed to block the detection DNA during the measurement, we abolish the recognition spots (Figure S 1d,e). Washing the substrate and tip with the PBS leads to recovery of the recognition signals to about the same level (Figure S1f, slightly different area after washing).

To quantify the binding affinity of target DNA, we applied varying target DNA concentrations. As is evident from the recognition images (Figure 3a,c), the number of recognition spots scales with increasing target DNA concentration. For further analysis, recognition spots are discerned through voltage grain analysis. We derived threshold images (Figure 3b,d) directly from the original recognition images by setting the threshold to the background noise (same value for all images) so as to arrive at a background-subtracted image for highlighting the selected recognition spots. The size of a recognition spot localizing a single target DNA can be directly obtained from magnifying the threshold recognition image (Figure 3b) and is about 10 nm × 10 nm. This value is comparable with previous TREC studies.[29,30] The locations of the recognition spots are stable in two consecutive images of the same area (Figure S2a,b) because the thermal drift is reduced in this fast scan speed. However, the shape of the spots slightly vary due to the probabilistic nature of the molecular binding and unbinding process during TREC imaging. We then directly counted the pixels that contained recognition signals when different concentrations of target DNA were used; the percentage of recognition pixels over the total image pixels increases from 3.6% to 22% at 1000 times higher concentrations (from 10 pM to 10 nM; see Table 2). Importantly, when we compare the detected recognition values between TREC (recognition pixels) and force-mapping measurements (cluster numbers) at different concentrations, we find a strong linear correlation (adjusted r^2 of 0.88, linear regression model, Figure 3e).

The performance of our method for determining the equilibrium dissociation constant was analyzed using the Langmuir model. The molecular binding reaction at equilibrium is represented through $[A] \times [B] \cdot k_{on} = [AB] \times k_{off}$, where, in our case, A is the capture DNA, B is the target DNA, and AB are the hybridized capture/target DNA complexes. Thus, the equilibrium dissociation constant K_D is defined as:

$$K_D = \frac{k_{off}}{k_{on}} = \frac{[A] \times [B]}{[AB]} \quad (1)$$

with k_{on} being the association rate and k_{off} being the dissociation rate.

If $[A] = K_D$, 50% of target DNA is bound to capture DNA. The amount of capture/target DNA hybridization can be fitted with the Langmuir model, as described below eq 2. The recognition areas represented as percentages were fitted in dependence on the target DNA concentration (Figure 3f and Table 2), which yields an equilibrium dissociation constant of $K_D = 2.4 \times 10^{-10}$ M (adjusted r^2 of 0.93):

$$y = \frac{abx^{1-c}}{1 + bx^{1-c}} \quad (2)$$

The change in equilibrium free energy is then estimated as per eq 3:

$$\Delta G = -RT \ln {}^{1}/_{K_D} \quad (3)$$

at 52 °C (hybridization temperature), resulting in a value of −14.3 kcal/mol.

The probe−target hybridization free energy was estimated with nearest-neighbor parameters derived from the nearest-neighbor model.[34,35] For our surface-bound DNA, we considered all possible 16 possible nearest-neighbor (NN) pairs (for example, 5′-AT-3′/3′-TA-5′ pair, 5′-TA-3′/3′-AT-5′

DOI: 10.1021/acs.nanolett.8b04883
Nano Lett. 2019, 19, 612−617

pair, 5′-AG-3′/3′-TC-5′ pair, 5′-GA-3′/3′-CT-5′ pair, etc.) typically used in solution. In addition, the binding interaction on the surface has been reported to be different, as the degree of freedom of the surface-tethered probe is restricted. This was accounted by the double-ended zipper model,[36,37] in which the probe−target pair can be viewed as a double-ended zipper with two unbound parts starting at both ends. Considering the fraction of the unbound part,[38] we eliminated the contribution from the respective NN pairs from both ends to the hybridization free energy, which amounts to a $\Delta G_{52\,^{\circ}C}$ value of −17.0 kcal/mol. This estimation is in close agreement with the experimentally observed value and validates our data obtained from recognition imaging.

Our study presents TREC-AFM as a powerful tool for label-free quantification affinity by localizing molecular recognition events at the nanoscale. We have applied our method for characterizing DNA arrays at the single DNA/DNA hybridization level. Compared to the force-mapping-based method, TREC achieved a faster recording time 50 times faster (4.25 min) with pixelation density 64 times higher (1.9 nm pixel size) when compared to force mapping (210 min, 15.6 nm pixel size). We revealed affinities from analyzing DNA arrays containing just 100−700 molecules. Other label-free surface detection methods such as SPR and QCM would require a minimum number of 10^4 and 10^7 of our target DNA molecules, respectively. TREC-AFM provides a fast and label-free biosensing platform for affinity studies with minute sample amounts. Applicable to any receptor/ligand combination, it might open new possibilities for alternative next-generation affinity sensors. Our approach is also compatible with cantilever arrays for parallel high-throughput analysis.

■ ASSOCIATED CONTENT

Supporting Information

The Supporting Information is available free of charge on the ACS Publications website at DOI: 10.1021/acs.nanolett.8b04883.

Additional details on the experimental methods and figures showing the specificity of recognition images and consecutive recognition images (PDF)

■ AUTHOR INFORMATION

Corresponding Author

*E-mail: peter.hinterdorfer@jku.at.

ORCID

Joon Won Park: 0000-0003-1432-3161

Peter Hinterdorfer: 0000-0003-2583-1305

Present Addresses

[§]Université Catholique de Louvain, Louvain-la-Neuve, Belgium

[∥]Department of Electrical Engineering, Columbia University, New York, NY 10027, United States

Author Contributions

Y.J.O., J.W.P., and P.H. designed the project. Y.J.O., M.K., and Y.L. performed the experiments and data analysis. Y.L. and S.M. developed the chemistry methods, produced samples, and provided force-mapping data. Y.J.O., J.W.P., and P.H. prepared the final manuscript. All authors discussed the results and commented on the manuscript.

Notes

The authors declare no competing financial interest.

■ ACKNOWLEDGMENTS

This study was funded by the Austrian Science Fund FWF projects I 3173, V 584-BBL, the Austrian National Foundation for Research, Technology and Development and Research Department of the State of Upper Austria, and the National Research Foundation of Korea (NRF-2016K2A9A1A03904662).

■ ABBREVIATIONS

AFM, atomic force microscopy;; ELISA, enzyme-linked immunosorbent assays; SPR, surface plasmon resonance; TREC, topography and recognition; QCM, quartz crystal microbalance

■ REFERENCES

(1) Schmidt, R.; Jacak, J.; Schirwitz, C.; Stadler, V.; Michel, G.; Marmé, N.; Schütz, G. J.; Hoheisel, J. D.; Knemeyer, J.-P. *J. Proteome Res.* **2011**, *10* (3), 1316−1322.

(2) McKendry, R.; Zhang, J.; Arntz, Y.; Strunz, T.; Hegner, M.; Lang, H. P.; Baller, M. K.; Certa, U.; Meyer, E.; Güntherodt, H.-J.; Gerber, C. *Proc. Natl. Acad. Sci. U. S. A.* **2002**, *99* (15), 9783−9788.

(3) Fredriksson, S.; Gullberg, M.; Jarvius, J.; Olsson, C.; Pietras, K.; Gústafsdóttir, S. M.; Östman, A.; Landegren, U. *Nat. Biotechnol.* **2002**, *20*, 473.

(4) Rissin, D. M.; Kan, C. W.; Campbell, T. G.; Howes, S. C.; Fournier, D. R.; Song, L.; Piech, T.; Patel, P. P.; Chang, L.; Rivnak, A. J.; Ferrell, E. P.; Randall, J. D.; Provuncher, G. K.; Walt, D. R.; Duffy, D. C. *Nat. Biotechnol.* **2010**, *28*, 595.

(5) Boutorine, A.; Novopashina, D.; Krasheninina, O.; Nozeret, K.; Venyaminova, A. *Molecules* **2013**, *18* (12), 15357.

(6) Hua, B.; Wang, Y.; Park, S.; Han, K. Y.; Singh, D.; Kim, J. H.; Cheng, W.; Ha, T. *Biochemistry* **2018**, *57* (10), 1572−1576.

(7) Lee, H.; Park, J.-E.; Nam, J.-M. *Nat. Commun.* **2014**, *5*, 3367.

(8) Su, X.; Wu, Y. J.; Robelek, R.; Knoll, W. *Langmuir* **2005**, *21* (1), 348−53.

(9) Höök, F.; Ray, A.; Nordén, B.; Kasemo, B. *Langmuir* **2001**, *17* (26), 8305−8312.

(10) Köβlinger, C.; Uttenthaler, E.; Drost, S.; Aberl, F.; Wolf, H.; Brink, G.; Stanglmaier, A.; Sackmann, E. *Sens. Actuators, B* **1995**, *24* (1), 107−112.

(11) Yao, C.; Zhu, T.; Qi, Y.; Zhao, Y.; Xia, H.; Fu, W. *Sensors* **2010**, *10* (6), 5859−71.

(12) Hinterdorfer, P.; Dufrêne, Y. F. *Nat. Methods* **2006**, *3*, 347.

(13) Dufrêne, Y. F.; Ando, T.; Garcia, R.; Alsteens, D.; Martinez-Martin, D.; Engel, A.; Gerber, C.; Müller, D. J. *Nat. Nanotechnol.* **2017**, *12*, 295.

(14) Preiner, J.; Horner, A.; Karner, A.; Ollinger, N.; Siligan, C.; Pohl, P.; Hinterdorfer, P. *Nano Lett.* **2015**, *15* (1), 759−763.

(15) Husale, S.; Persson, H. H. J.; Sahin, O. *Nature* **2009**, *462*, 1075.

(16) Medalsy, I.; Hensen, U.; Muller, D. J. *Angew. Chem., Int. Ed.* **2011**, *50* (50), 12103−12108.

(17) Rico, F.; Su, C.; Scheuring, S. *Nano Lett.* **2011**, *11* (9), 3983−3986.

(18) Florin, E. L.; Moy, V. T.; Gaub, H. E. *Science (Washington, DC, U. S.)* **1994**, *264* (5157), 415−7.

(19) Hinterdorfer, P.; Baumgartner, W.; Gruber, H. J.; Schilcher, K.; Schindler, H. *Proc. Natl. Acad. Sci. U. S. A.* **1996**, *93* (8), 3477−3481.

(20) Lee, G. U.; Chrisey, L. A.; Colton, R. J. *Science (Washington, DC, U. S.)* **1994**, *266* (5186), 771−3.

(21) Oh, Y. J.; Hubauer-Brenner, M.; Gruber, H. J.; Cui, Y.; Traxler, L.; Siligan, C.; Park, S.; Hinterdorfer, P. *Sci. Rep.* **2016**, *6*, 33909.

(22) Rief, M.; Gautel, M.; Oesterhelt, F.; Fernandez, J. M.; Gaub, H. E. *Science (Washington, DC, U. S.)* **1997**, *276* (5315), 1109−1112.

(23) Marszalek, P. E.; Lu, H.; Li, H.; Carrion-Vazquez, M.; Oberhauser, A. F.; Schulten, K.; Fernandez, J. M. *Nature* **1999**, *402*, 100.

DOI: 10.1021/acs.nanolett.8b04883
Nano Lett. 2019, 19, 612−617

(24) Yee, K.; Anglin, P.; Keating, A. *Blood Rev.* **1999**, *13* (2), 105−126.
(25) Hong, B. J.; Sunkara, V.; Park, J. W. *Nucleic Acids Res.* **2005**, *33* (12), e106−e106.
(26) Mishra, S.; Lee, Y.; Park, J. W. *Anal. Chem.* **2018**, *90* (21), 12824−12831.
(27) Lee, Y.; Kim, Y.; Lee, D.; Roy, D.; Park, J. W. *J. Am. Chem. Soc.* **2016**, *138* (22), 7075−7081.
(28) Lee, Y.; Kwon, S. H.; Kim, Y.; Lee, J. B.; Park, J. W. *Anal. Chem.* **2013**, *85* (8), 4045−50.
(29) Stroh, C.; Wang, H.; Bash, R.; Ashcroft, B.; Nelson, J.; Gruber, H.; Lohr, D.; Lindsay, S. M.; Hinterdorfer, P. *Proc. Natl. Acad. Sci. U. S. A.* **2004**, *101* (34), 12503−12507.
(30) Stroh, C. M.; Ebner, A.; Geretschläger, M.; Freudenthaler, G.; Kienberger, F.; Kamruzzahan, A. S. M.; Smith-Gill, S. J.; Gruber, H. J.; Hinterdorfer, P. *Biophys. J.* **2004**, *87* (3), 1981−1990.
(31) Raab, A.; Han, W.; Badt, D.; Smith-Gill, S. J.; Lindsay, S. M.; Schindler, H.; Hinterdorfer, P. *Nat. Biotechnol.* **1999**, *17* (9), 901−5.
(32) Chtcheglova, L. A.; Waschke, J.; Wildling, L.; Drenckhahn, D.; Hinterdorfer, P. *Biophys. J.* **2007**, *93* (2), L11−L13.
(33) Preiner, J.; Ebner, A.; Chtcheglova, L.; Zhu, R.; Hinterdorfer, P. *Nanotechnology* **2009**, *20* (21), 215103.
(34) Breslauer, K. J.; Frank, R.; Blöcker, H.; Marky, L. A. *Proc. Natl. Acad. Sci. U. S. A.* **1986**, *83* (11), 3746−3750.
(35) Sugimoto, N.; Nakano, S.-i.; Katoh, M.; Matsumura, A.; Nakamuta, H.; Ohmichi, T.; Yoneyama, M.; Sasaki, M. *Biochemistry* **1995**, *34* (35), 11211−11216.
(36) Binder, H. *J. Phys.: Condens. Matter* **2006**, *18* (18), S491.
(37) Kittel, C. *Am. J. Phys.* **1969**, *37* (9), 917−920.
(38) Deutsch, J. M.; Dhar, A.; Narayan, O. **2004**, *arXiv:q-bio/0406039 [q-bio.BM]*. arXiv.org e-Print archive. https://arxiv.org/abs/q-bio/0406039 (accessed June 28, 2018)
(39) Oh, S. J.; Ju, J.; Kim, B. C.; Ko, E.; Hong, B. J.; Park, J.-G.; Park, J. W.; Choi, K. Y. *Nucleic Acids Res.* **2005**, *33* (10), e90−e90.

DOI: 10.1021/acs.nanolett.8b04883
Nano Lett. 2019, 19, 612−617